JOC The Journal of Organic Chemistry

Featured Article

pubs.acs.org/joc

Nonclassical CH−π Supramolecular Interactions in Artemisinic Acid Favor a Single Conformation, Yielding High Diastereoselectivity in the Reduction with Diazene

Bertrand Castro,*[,†] Robin Chaudret,*[,‡,#] Gino Ricci,[§] Michael Kurz,[∥] Philippe Ochsenbein,[⊥] Gerhard Kretzschmar,[∥] Volker Kraft,[∥] Kai Rossen,[∥] and Odile Eisenstein*[,†]

[†]Institut Charles Gerhardt, CNRS 5253, Université Montpellier 2, cc 1501, place E. Bataillon, F-34095 Montpellier, France

[‡]IFP Energies Nouvelles, 1 et 4 avenue de Bois-Préau, 92852 Rueil-Malmaison Cedex, France

[§]Sanofi Chimie, 45 chemin de Meteline 04200 Sisteron, France

[∥]Sanofi-Aventis Deutschland GmbH, Chemistry & Biotechnology Department, Industriepark Höchst, D-65926 Frankfurt am Main, Germany

[⊥]Sanofi-Aventis R & D, 371 rue du Professeur Joseph Blayac, 34184 Montpellier Cedex 04, France

Supporting Information

ABSTRACT: The high diastereoselectivity of the hydrogenation of artemisinate by diazene to form dihydroartemisinate (diastereoselective ratio, dr, 97:3) necessary for efficient production of artemisin has been rationalized by state-of-the-art DFT calculations and identification of the noncovalent interactions by coupled ELF/NCI analysis. Remarkably, a single conformer of artemisinate is responsible for the high diastereoselectivity of the reaction. NMR studies confirm the preference for a single conformation that is found to be identical to that predicted by the calculations. The calculations and ELF/NCI analyses show that the hydrogenation of the exocyclic activated C=C double bond has a low energy barrier and that the lowest transition state and the preferred conformation of free artemisinate develop the same network of weak noncovalent interactions between the electron donor groups (oxygen and exocyclic C=C double bond) and CH bonds of the *cis*-decalene group of the artemisinate, which rationalize the high diastereoselectivity unusual for a strongly exothermic reaction.

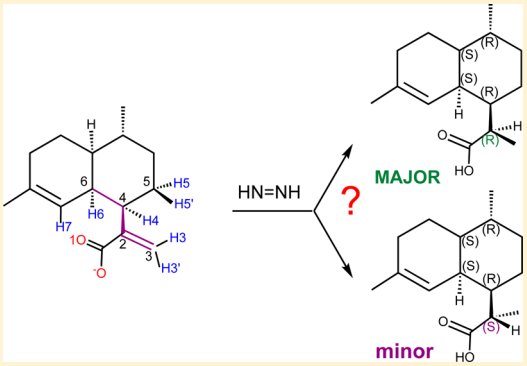

INTRODUCTION

Asymmetric synthesis is a key topic for organic chemistry. Numerous studies have been devoted to establish and understand the factors that control the diasterostereoselective ratio, dr.[1−4] As stated in one of the articles in the *Chemical Reviews* issue devoted to asymmetric induction, "Beyond any doubt the best-documented and most powerful factor is the steric one...it is virtually always taken for granted that the selectivity is the result of a difference in steric hindrance between the two approaches the reagent may choose".[3] However, other factors may play a role as highlighted by the earliest theoretical analyses based on molecular orbital considerations.[4] Nevertheless, the successful manipulation of steric effects has been at the heart of the development of catalysts, such as for hydrogenation. A number of transition-metal complexes based notably on Rh and Ru metals have been found to give highly satisfactory results in asymmetric hydrogenation,[5−7] and ligand optimization and theoretical studies have highlighted the importance of steric effects in controlling the diastereoselectivity.[8−10] The lowest transition state, leading to the major diastereomeric product, corresponds to a geometrical configuration where steric effects (always supposed to be destabilizing) between the reactive species are minimized. A consequence of the determining influence of steric factors is that, in general, the dr is enhanced by bulky groups in the two reactants because they increase the energy difference between the preferred and less preferred configurations.

For this reason, the discovery that reduction of artemisinic acid, **1**, to dehydroartemisinic acid, **2**, gives high dr (97:3) when reacting with diazene, HN=NH, appears as a remarkable paradox.[11,12] The hydrogenation of the exocyclic double bond is expected to occur with at most very small dr. While the olefin is attached to a *cis*-decalene group with four chiral centers, it can rotate freely about the C2−C4 single bond because no bulky group is present to hinder the rotation. In addition to the absence of steric factors, the bicyclic group carries no functional group other than an intracyclic C=C double bond. Consequently, no interaction is expected between the *cis*-

Received: January 31, 2014
Published: March 10, 2014

   dx.doi.org/10.1021/jo500233z | J. Org. Chem. 2014, 79, 5939−5947

decalene derivative and the exocyclic conjugated carboxylic acid. This should lead to no conformational preference in **1**. Therefore, a conventional analysis suggests that the hydrogenation of **1** by diazene should not be selective. However, it is now well established that CH bonds engage in weak stabilizing interactions with electron-rich groups such as lone pairs on X atoms (X = O, N etc.), or C=C π bonds,[13,14] for which computations have highlighted the role of dispersion.[15] Similar considerations have been developed for interactions between CH/CH bonds.[16] These noncovalent interactions, which are weaker than traditional hydrogen bonds, have been called nonclassical hydrogen bonds. These interactions, which contribute each little to the global intra- or intermolecular interactions, can sum up to significant interaction energies because of the large number of them in most chemical systems. All together, they are known to contribute to conformation of molecules, specificity of molecular recognition, selectivity in organic reactions, polymer science, surface phenomema, and interactions with proteins.[15] The major difficulty in analyzing the structure of a chemical system determined by an ensemble of noncovalent interactions is that there is no obvious hierarchy among them. Consequently, it is difficult to predict the best network of an ensemble of weak interactions and a computational approach is needed to give insights.

In this work, we present a computational study of the diastereoselective hydrogenation of artemisinic acid by diazene that reproduces essentially quantitatively the surprisingly high diastereoselective ratio of 97:3. The calculations show that few transition states for the addition of diazene to **1** essentially determine the observed dr and that the major diastereomer is obtained through a single transition state associated with a well-defined conformation of the artemisinic acid. The factors that favor this conformation and their necessary relationships with the low energy barrier of the hydrogenation by diazene are presented. This computational study leads to the unexpected suggestion that artemisinic acid has a preferred conformation determined by a network of weak nonclassical CH interactions. The conformation predicted by the calculations is validated by a solution NMR study of **1**, in the experimental conditions of the hydrogenation reaction. This study suggests that the ensemble of weak forces can add up significantly and may present a novel approach for asymmetric catalyst development.

EXPERIMENTAL BACKGROUND

The hydrogenation of artemisinic acid (**1**) to dihydroartemisinin is part of an important effort to develop an efficient and cost-effective synthetic route to form artemisinin **3** on a large scale, adapted to the need to provide this potent antimalaria drug. The only natural source of artemisinin is the plant *Artemisia annua*, which produces artemisinin in poor and highly variable yield (0.001−0.8% from the dry plant). Consequently, an efficient synthetic route to artemisinin is needed. While several total syntheses of artemisinin are known,[17−22] none of them is suitable for the required large scale and low cost preparation. The most efficient access to artemisinin, set up by Amyris Biotechnologies Inc., and developed in collaboration by Sanofi,[23] involves a fermentative access to the intermediate artemisinic acid, which contains the complete carbon skeleton of artemisinin, followed by a sequence of chemical transformations to artemisinin.[23−27] As shown in Scheme 1, the sequence commences with the hydrogenation of artemisinic acid (**1**) to dehydroartemisinic acid (**2a**), which is subsequently biomimetically oxygenated to artemisinin (**3**).[21,22,28]

Scheme 1. Key Steps of the Synthesis of Artemisinin with Diazene

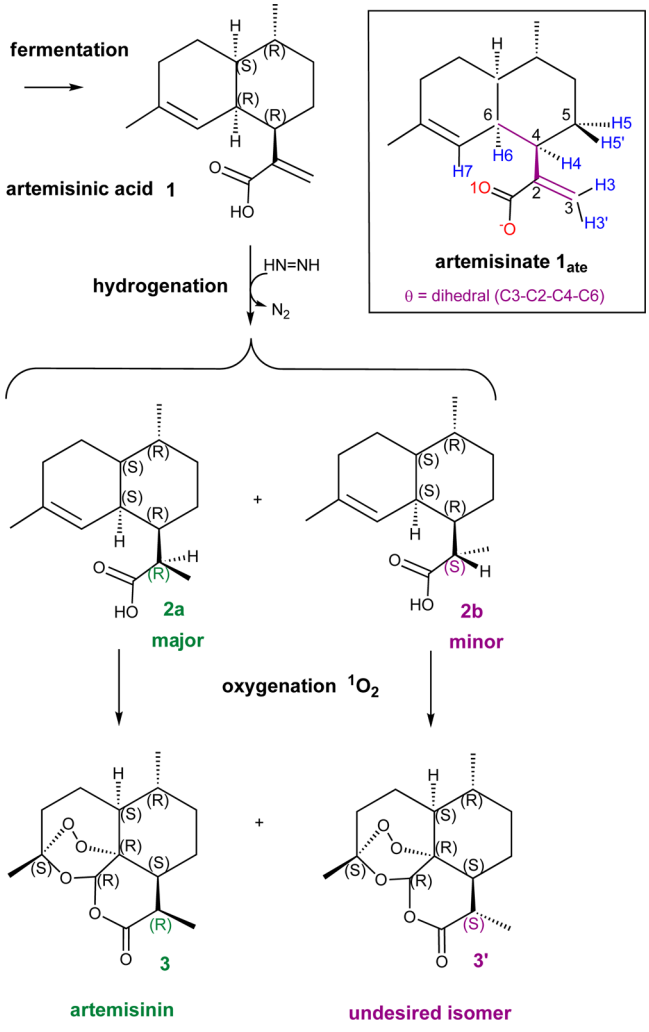

A high selectivity of the hydrogenation of **1** to **2a** is the required key factor for an economical and clean total synthesis. Although the preferential formation of the diastereoisomer with an R configuration at C_2, **2a**, is well documented for any achiral reductant, the crucial diastereoselectivity of this step was not fully addressed in previous publications.[29−35] Our search for a highly diastereoselective hydrogenation prompted us to examine diazene, NH=NH. While known for a long time,[36,37] hydrogenation by diazene is only occasionally used in synthesis and has been essentially ignored for industrial applications, possibly because of the reputed safety issues. Indeed, diazene is not stable and needs to be generated in situ. A practical and safe implementation based on the addition of hydrazine and H_2O_2 or air to an alcoholic solution of **1** at 0 °C at pH 9 was identified. This diazene, generated in situ, hydrogenates **1** to **2** with a remarkably high diastereoselectivity ratio, dr, **2a**:**2b** of 97:3 and regio extracyclic selectivity of over 99:1. This method produced the desired "R isomer" **2a** without any need for chromatography or selective crystallization and, most remarkably, without a need for an external catalyst. This process is demonstrated on a large scale by SANOFI and appears to be a viable solution to the desired efficient synthetic route to artemisinin.[11,12] As mentioned earlier, the reasons of this high diastereoselectivity are unclear and it is paradoxical

dx.doi.org/10.1021/jo500233z | J. Org. Chem. 2014, 79, 5939−5947

Table 1. Transition States of Hydrogenation of the Exocyclic C=C Double Bond of Artemisinate $\mathbf{1}_{ate}$ by Diazene To Form 2a and 2b (See Scheme 1 for the Definition of θ)

entry	diastereomeric transition state	associated product	θ (deg)	$\Delta G^{\ddagger a}$ (kcal/mol)	$\Delta\Delta G^{\ddagger}$ (kcal/mol)	2a:2b
1	*pro-R*	**2a**	−94.0	7.9	0.0	92.8
2			9.5	9.7	1.80	3.4
3			131.0	11.7	3.80	0.1
4	*pro-S*	**2b**	−165.0	11.2	3.3	0.2
5			−70.0	10.2	2.3	1.5
6			71.0	10.0	2.1	2.1

[a]Free energies relative to the separated reactants: $\mathbf{1}_{ate}$ (θ = −109°, global minimum) and diazene.

that such a high dr is achieved in a fast, exothermic reaction where potentially controlling steric factors are absent.

COMPUTATIONAL DETAILS

All structures were optimized with the DFT method at the B3LYP level[38,39] with a 6-311G(d,p) basis set for all atoms. The nature of all extrema as minimum or transition state was characterized with analytical calculations of frequencies, and the transition states were connected to reactants and products with IRC calculations. To reproduce the experimental conditions (pH = 9), the conjugated base $\mathbf{1}_{ate}$ of **1** was considered as the reactive species. Test calculations indicate that results are similar with the artemisinic acid. Dispersion correction at the B3LYP-D3[40] level was added as single-point calculations on the B3LYP-optimized extrema. The effect of the solvent (MeOH) was included carrying out single-point calculations with the SMD method.[41] The gas-phase free energies were calculated using the harmonic approximation of frequencies at the experimental temperature of 273 K. The Gibbs energy profiles presented in this work are obtained by adding the free energy correction calculated in the gas phase to the energies calculated in solution corrected by the contribution from the dispersion contribution.[42] Calculations were carried out using the Gaussian 09 suite of programs.[43] The network of interactions was identified using both the electron localization function (ELF),[44,45] which defines the probability to find electrons of opposite spins, and the noncovalent interaction (NCI) index, which defines the regions of weak attractive or repulsive interactions.[46] Additional information on these two methods is given in the Supporting Information. The previous analyses were performed using the TopMod[47] and NCIplot[48] softwares, respectively, with default values presented in the corresponding software. For all graphics, the following cutoffs were used: ELF < 0.86 for ELF and RDG < 0.4 and $-0.02 < \lambda_2{*}\rho < 0.02$ for NCI. It should be noted that in the case of ELF the volume of the basin is not directly related its population. The population analysis obtained through integration using the TopMod program are given in the Supporting Information. These methods have been used to identify interactions in a wide variety of chemical and biochemical systems.[48−52] Furthermore, the use of these two approaches together was recently shown to give insights into the evolution of the interaction during a chemical reaction.[53,54]

RESULTS

1. Conformational Preferences of $\mathbf{1}_{ate}$. The reaction is run in MeOH solution, and the hydrogenation is carried at pH 9, where the artemisinic acid is deprotonated. To properly represent these experimental conditions, the calculations were carried out for the artemisinate anion in MeOH solution. As shown on Scheme 1, artemisinate has limited conformational freedom since the junction in the bicyclic ring is fixed, as well as the position of the intracyclic double ring, and the exocyclic carboxylate group can only occupy an equatorial site at C4. Consequently, the geometry of $\mathbf{1}_{ate}$ is fully defined by the orientation of the exocyclic group relative to the cis-decalene group, which is described by the θ dihedral angle C3−C2−C4−C6. Geometry optimizations of free artemisinate reveal the presence of three minima. The most stable conformation is for θ equal to −109°, and the two secondary minima, 3.3 and 3.8 kcal/mol above the global minimum, correspond to θ values of 0° and 94°, respectively. The transition states (TS) for the rotation of the exocyclic group were located for θ = 36, 161, and −50° at Gibbs energies of 5.8, 6.4, and 5.9 kcal/mol above the global minimum, respectively. These barriers of rotation of less than 6 kcal/mol suggest a slightly hindered rotation about the C2−C4 bond compatible with the absence of any short distances between nonbonded atoms. Considering the energy pattern that has been obtained, free artemisinate should be mostly in the θ = −109° conformation.

2. Transition States for the Addition of Diazene to Artemisinate. Experimental studies have shown that *Z*-diazene hydrogenates an olefin in a cis manner with high selectivity, suggesting a concerted transfer of the two hydrogen atoms.[55−58] This reaction, in which two hydrogen atoms are transferred from HA−AH to A=A or B=B (A, B = C, N, or O), known as a dyotropic reaction of type 2, has attracted considerable interest from the theoretical community.[59] Experimental studies have shown that the hydrogenation by diazene is a facile reaction and computational studies with methods including electronic correlation have found low energy barriers.[60−63]

The conformations of $\mathbf{1}_{ate}$ that correspond to the three minima for the isolated molecules were used for initial search of the transition states for the hydrogenation by diazene, which is considered in its *Z*-reactive structure. For each conformation of $\mathbf{1}_{ate}$, HN=NH was positioned on either side of the C=C exocyclic double bond and a full geometrical search of the transition states was conducted without any constraint. For each conformation, only one of the two diastereotopic approaches was found to give an accessible transition state. To identify other possible transition states associated with other conformations of $\mathbf{1}_{ate}$, the dihedral angle was changed by up to 30° relative to the three previously studied conformations and a full search of transition state was conducted. This systematic procedure led to the six transition states shown in Table 1; three of them yield **2a** (the desired diastereoisomer) and three of them **2b** (the undesired one). Since the configuration of the new chiral carbon center is R in **2a** and S in **2b**, the three first transition states are also called *pro-R* and the other ones are called *pro-S*. Each of these transition states is fully identified by the value of θ and its *pro-R*/*pro-S* characteristics.

The six transition states have essentially identical geometrical parameters for the six atoms (N, H, and C) describing the hydrogen transfer reaction. The six atoms are coplanar, and the interatomic distances are as follows: NH, 1.16 Å; H···C4, 1.54 Å; H···C3, 1.60 Å; C2−C3, 1.39 Å; and N−N, 1.19 Å. These geometrical parameters are reasonably close to those obtained for the MP2 calculations of the transition state for the

dx.doi.org/10.1021/jo500233z | J. Org. Chem. 2014, 79, 5939−5947

hydrogenation of ethylene by diazene for which NH is 1.123 Å, H···C is 1.707 Å, CC is 1.372 Å, and NN is 1.233 Å.[63] The geometry of the transition state of this concerted reaction is thus reactant like for $\mathbf{1}_{ate}$ since the C2−C3 bond distance of the double bond increases only from 1.38 to 1.39 Å. Geometrical changes are larger in diazene where the NN bond distance shortens significantly from 1.23 in free diazene to 1.19 Å at the transition state. The reaction has low activation barriers ($\Delta G^{\ddagger}$ from 7.9 to 11.7 kcal mol^{-1}, depending on θ) and a large energy of reaction ($\Delta G = -65$ kcal mol^{-1}) as it forms N_2. These values are compatible with a rapid reaction as found for fumaric acid olefins.[61] This is also in agreement with the overall rapid reaction observed in the case of artemisinic acid, although no detailed kinetics could be carried out.

Since the six transition states have similar geometrical features for the six atoms involved in N−H and C−H bond breaking and making, their different energies are caused by the difference in the orientation of the cis-decalene group relative to the exocyclic conjugated carboxylate, described by the dihedral angle θ. The contribution of the six transition states to the formation of **2a** and **2b** is estimated by a Boltzmann distribution calculated at 273 K. Entries 1−3 yield **2a** and entries 4−6 yield **2b** leading to a ratio **2a**:**2b** of 96:4, which agrees well with the observed dr of 97:3. Furthermore, a single transition state (entry 1) is responsible for the massive production of **2a** while the formation of **2b** is more equally distributed over two transition states (entries 5 and 6). In entries 1 and 6, the diazene is far from the *cis*-decalene group, and thus, the energy difference between these two entries does not involve interactions between the diazene and the *cis*-decalene, which is the group that transfers chirality. In contrast, in entry 5, the diazene is relatively close to the *cis*-decalene. Consequently, the energy of this later transition state involves the interaction between the diazene and the *cis*-decalene. The purpose of this study is to analyze why entry 1 is so much favored relative to entries 5 and 6. We thus focus on the comparison between entries 1 and 6 which share the remarkable property to have no interaction between the incoming reactant and the *cis*-decalene group transferring chirality and which can be meaningfully compared.

3. Comparison between the Representative *pro-R* and *pro-S* Transition States. For entries 1 and 6, the θ angle is −94° and 71°, respectively. These two values of θ are relatively close to −109° and 90°, which are associated with the preferred conformation and a secondary minimum of free artemisinate, respectively. Thus, the two lowest transition states that control the stereoselectivity of the hydrogenation of $\mathbf{1}_{ate}$ by diazene are obtained for values of θ that are close to those that minimize the energy of free $\mathbf{1}_{ate}$. In the case of free $\mathbf{1}_{ate}$, the two minima (θ = −109° and 90°) differ by 3.8 kcal/mol, while the two transition states (entries 1 and 6) differ by 2.0 kcal/mol. This suggests that the factors that make the *pro-R* TS of entry 1 lower than the *pro-S* TS of entry 6 are similar to those that make the (θ = −109°) conformation more stable than (θ = 90°). To put this onto more quantitative ground, the energy barriers for the transition states associated with entries 1 and 6 are analyzed using the thermodynamic cycle of Scheme 2 with numerical values given in Table 2. Each energy barrier (not the free energy barrier) is decomposed into distortion energies and interaction energies. The distortion energy evaluates the energy cost to bring each chemical species from its structure in the isolated system to that in the transition state. The interaction energy evaluates the interaction between the two distorted

Scheme 2. Decomposition of the Energy Barrier for the Reaction between $\mathbf{1}_{ate}$ and Diazene[a]

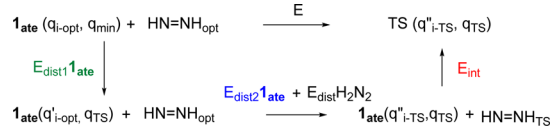

[a] q, q', and q'' are the internal coordinates of $\mathbf{1}_{ate}$ other than the dihedral θ angle.

Table 2. Decomposition of the Energy Barriers (kcal/mol)[a]

	pro-R		*pro-S*	
component	θ (°)	E	θ (°)	E
$\Delta E^{\ddagger}$[b]	−94	5.0[c]	90	3.2[d]
$E_{dist1}\mathbf{1}_{ate}$	−109 → −94	0.2	90 → 71	0.10
$E_{dist2}\mathbf{1}_{ate}$	−94	7.00	71	6.1
$E_{dist}H_2N_2$	−94	15.5	71	14.6
$\sum(E_{dist})$	−94	22.7	71	20.8
E_{int}	−94	−17.7	71	−17.6
energy $\mathbf{1}_{ate}$[c]	−109	0.0	90	3.8
energy TS[c]	−94	5.0	71	7.0

[a] See Scheme 2 for notations. [b] Energy barrier relative to $\mathbf{1}_{ate}(\theta)$. [c] Energy relative to $\mathbf{1}_{ate}$ (−109°). [d] Energy relative to $\mathbf{1}_{ate}$ (90°).

species. In the present case, the distortion energy of $\mathbf{1}_{ate}$, E_{dist}-$\mathbf{1}_{ate}$, is divided into two parts, $E_{dist1}\mathbf{1}_{ate}$ and E_{dist2}-$\mathbf{1}_{ate}$. For obtaining $E_{dist1}\mathbf{1}_{ate}$, $\mathbf{1}_{ate}$ is distorted from its optimized geometry ($\mathbf{1}_{ate}(q_{i\text{-}opt}, \theta_{min})$ to a geometry where only the θ angle is changed from its value in the isolated species to its value at the transition state, all other structural parameters being reoptimized, $\mathbf{1}_{ate}(q'_{i\text{-}opt}, \theta_{TS})$. For obtaining E_{dist2}-$\mathbf{1}_{ate}$, $\mathbf{1}_{ate}$ is distorted from $\mathbf{1}_{ate}(q'_{i\text{-}opt}, \theta_{TS})$ to the geometry in the TS, $\mathbf{1}_{ate}(q''_{i\text{-}TS}, \theta_{TS})$. The value of E_{dist1}-$\mathbf{1}_{ate}$ is small, which indicates that there is no energy cost in changing the conformation of free artemisinate in the range of values of θ (−109 to −94° and 90 to 71, for the *pro-R* and pros S species, respectively).

The values for further distortion of the artemisinate, E_{dist2}-$\mathbf{1}_{ate}$, and diazene, E_{dist}-H_2N_2, are similar for the *pro-R* and *pro-S* transition states although slightly lower (ca. 2 kcal/mol) for the latter. The energies of interaction are essentially identical for the two transition states. This makes the two energy barriers, measured from the energy of their corresponding conformers, rather similar although slightly lower for the *pro-S* TS. Consequently, the transition state of entry 1 is lower than that of entry 6 because the conformation of isolated artemisinate for θ = −109° is more stable than that for θ = 90°.

4. Factors Controlling the Conformational Preference in Artemisinate. To gain insight into the factors that favor the conformation with θ = −109° and the corresponding *pro-R* transition state with θ = −94°, the nature of the interactions between noncovalently bonded atoms was analyzed using NCI/ELF approach. The ELF analysis allows visualization of strong density regions and divides the molecular space into subregions called basins. The latter are represented here as gray volumes and have a chemical meaning since they represent single or double covalent bonds, lone pairs, atomic centers. The NCI index represents the reduced density gradient (RDG) as a function of the density and reveals the localization and the strength of the noncovalent interactions. Coupling ELF and NCI analyses gives information across the whole range of

dx.doi.org/10.1021/jo500233z | J. Org. Chem. 2014, 79, 5939−5947

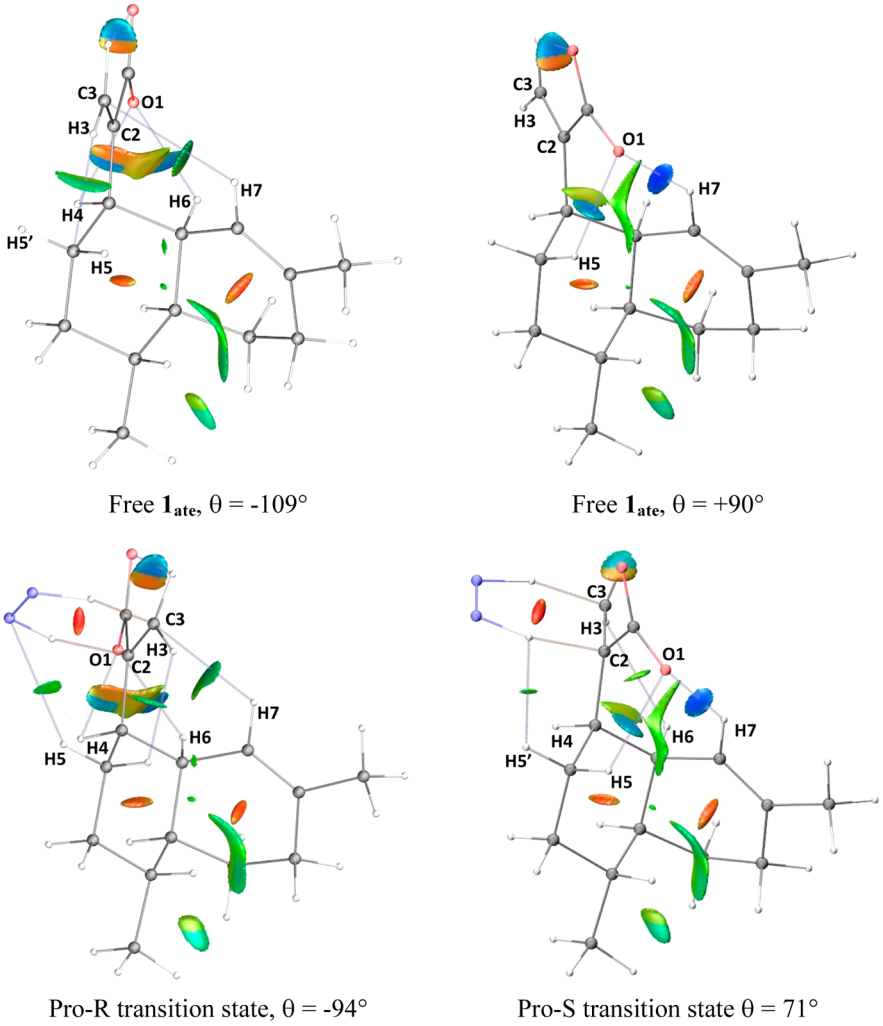

Figure 1. Color-coded noncovalent interactions (NCI) surfaces (blue strongly attractive, green weakly attractive, yellow and red repulsive) with lines indicating interacting atoms for two conformations of $\mathbf{1}_{ate}$ and two transition states for hydrogenation of $\mathbf{1}_{ate}$ by diazene (the cutoff values are RDG < 0.4 and $-0.02 < \lambda_2{*}\rho < 0.02$; see the Computational Details and Supporting Information for further information). Top: $\mathbf{1}_{ate}$, left/right ($\theta = -109°$, 90°). Bottom: transition states, left *pro-R* ($\theta = -94°$, entry 1), right *pro-S* ($\theta = 71°$, entry 6). The atom color codes are as follows: gray for C; white for H; red for O; blue for N. Carbon numbering, which is not shown, is identical to that of the hydrogen atoms (Hi is bonded to Ci).

interactions that control structure and chemical transformations, going all the way from strong to weak. In what follows, the weak interactions revealed by the NCI analysis are color coded from blue for strongly attractive weak interactions (hydrogen bonds, for example) to red for repulsive ones (steric clashes). In between, the very weak van der Waals interactions appear in green.

The NCI/ELF analyses for the two conformations, $\theta = -109°$ and 90° of isolated $\mathbf{1}_{ate}$ and for the lowest *pro-R* ($\theta = -94°$) and the selected *pro-S* ($\theta = 71°$) transition states, are presented in Figures 1 and 2 (full size graphics are included in the Supporting Information). The interactions invariant relative to θ do not need to be considered. Therefore, the analysis focuses on the through-space interactions between the conjugated carboxylate group and the cis-decalene ring. Lines connecting interacting atoms are drawn for facilitating the visual identification when needed. The presence of these interactions is confirmed by a decrease of the volume of the ELF basins of atoms and groups involved (Supporting Information).

Figure 1 shows that interactions occur between (i) O1 and (H4, H6), (ii) the C2═C3 bond and vinylic H7, and (iii) H3

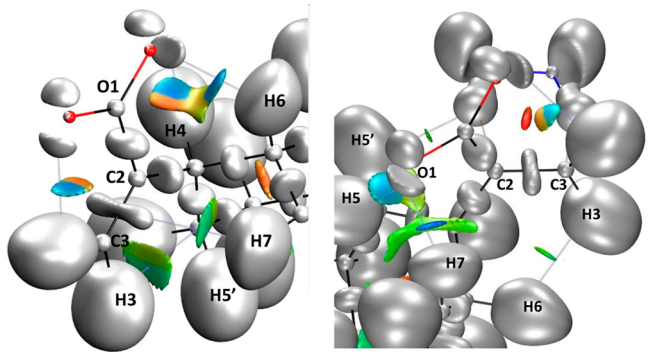

Figure 2. ELF volumes (gray) and NCI surfaces of the interactions on the labeled atoms of $\mathbf{1}_{ate}$ for left/right (θ: −109, 90°). Lines connect selected interacting groups (left: $\pi_{C2=C3}$ /H7C7, right O1/H7C7). For carbon numbering, see Figure 1. The cutoff values are ELF < 0.86, RDG < 0.4 and $-0.02 < \lambda_2{*}\rho < 0.02$. See the Computational Details and Supporting Information for further information.

dx.doi.org/10.1021/jo500233z | J. Org. Chem. 2014, 79, 5939−5947

and H5−H5′, for $\theta = -109°$. The ELF approach allows a visualization of the electronic densities involved in the interactions (Figure 2): (i) the interactions between O1 and (H4, H6) involve an oxygen lone pair and the tertiary H4C4 and H6C6 bonds as O···HC nonclassical interactions; (ii) the interaction between the C2═C3 bond and H7C7 involves the π density of the C2−C3 double bond and the vinylic H7C7 bond. For $\theta = 90°$, NCI analysis identifies noncovalent interactions between O1 and the vinylic H7C7 bond as well as the tertiary H5C5 bond. No CH bond is found to interact with the C2═C3 π density in this conformation.

In the two conformations several noncovalent interactions involving the vinylic and tertiary HC bonds and the oxygen and C═C double bond, as electron-rich groups, occur between the *cis*-decalene ring and the conjugated carboxylate group. Even though the methodology of identification of these interactions does not provide quantitative information on their energetic, the color code informs on their relative strength. Not surprisingly, the strongest interaction is between the oxygen and the vinylic H7C7 bond, as it occurs in $\mathbf{1}_{ate}$ for $\theta = 90°$, since it is shown as a deep blue surface while all other interactions are indicated as green surfaces (Figure 1). It is currently accepted that the oxygen lone pair is a stronger electron donor than the C2═C3 π bond. Likewise, a vinylic HC bond, which is more acidic than a tertiary HC bond, is associated with a stronger X··· HC interaction. Therefore, the calculations reveal that the most stable conformation ($\theta = -109°$) is not associated with the strongest O···H7C7 interaction. In contrast, the most stable conformation is associated with several interactions involving the O atom and the $\pi_{C2=C3}$ bond with tertiary (H4C4 and H6C6) and vinylic H7C7 bond, respectively. It thus appears that a larger stabilization involves *all* electron-rich groups into X···HC interactions. Considering the role of the geometry on these individual interactions, it is challenging and unlikely to determine a priori the network of weak interactions that is associated with the most stable conformation and a computational study is required for this determination.

A similar analysis is carried out for the *pro-R* and *pro-S* transition states (Figure 1, bottom). For the *pro-R* TS ($\theta = -94°$), the two noncovalent interactions that are identified for isolated $\mathbf{1}_{ate}$ at ($\theta = -109°$) are also present: (i) O1 interacts with tertiary H4C4 and H6C6 bonds and (ii) the π density of C2═C3 interacts with the vinylic H7C7 bond. However, the rotation of θ from −109° to −94° modifies the interactions between H3C3 and (H5C5, H5′C5). This weak interaction between HC bonds is reorganized to maintain an interaction between H3C3 and H5C5 and to form a new interaction between the N═N π system and H5′C5. Thus, even though there is some modification in the noncovalent interactions, the main interactions involving the more potent electron-donor groups (O1 and C2═C3), found in the $\theta = -109°$ conformation, are present at the *pro-R* TS. In the case of the *pro-S* TS, the NCI approach identifies the interactions between O1 and H7C7 and H5C5, which are present in isolated $\mathbf{1}_{ate}$ for $\theta = 90°$ and also some interactions between CH bonds (H7C7, H5C5). This confirms the analysis originating from the energy decomposition, i.e., the main noncovalent interactions that make the conformation ($\theta = -109°$) more stable than ($\theta = 90°$) for $\mathbf{1}_{ate}$ also makes the *pro-R* transition state, which forms **2a**, more stable than the *pro-S* transition state, which forms **2b**. The ELF analysis confirms that the noncovalent interactions have similar strengths in the ground and transition states (Supporting Information). In addition, NCI as well as ELF analyses find that the interactions associated with the newly made bonds, H8···C2 and H9···C3, are similar in the two transition states. This is also in agreement with the energy decomposition analysis; the two transition states do not differ by the way the C2═C3 bond interact with the diazene but by weak noncovalent interaction associated with the conformations of the artemesinate. The energy difference between the two transition states is thus a property of the isolated substrate. This result leads to a solution NMR study of artemisinate to test if this substrate assumes a dominating conformation as the computational studies suggest.

4. NMR Study of the Artemisinate. The computational study suggests that one conformation of artemisinate should dominate. In order to confirm the calculated structure, a conformational analysis based on NMR-derived interproton distances and restrained molecular modeling calculations has been performed. To reproduce the experimental conditions of the chemical reaction, the NMR experiments have been acquired using a sample of 6 mg of artemesinate dissolved in 600 μL of MeOD-d_4. The carboxyl function has been deprotonated by adding 5 mg of a 40% sodium hydroxide solution in D_2O. Based on 1D-^{1}H, 1D-^{13}C, DQF-COSY, NOESY, multiplicity edited-HSQC, and HMBC spectra, a complete assignment of proton and carbon chemical shifts has been achieved (see Table S1, Supporting Information).

From the NOESY spectrum, 18 distance constraints have been extracted which were used as input for a molecular dynamics calculation and energy minimization (for details, see the Supporting Information). Only one out of 18 distance constraints showed a small violation of 0.04 Å (see Table S2, Supporting Information). As expected, the conformation of the bicyclic core is essentially rigid. The proton $H12_{trans}$ (trans with respect to the carboxylate function) experiences two intensive NOEs to $H7_{ax}$ and $H7_{eq}$, which correspond to inter proton distances of 2.36 and 2.49 Å, respectively (see Figure S4, Supporting Information). These constraints lead to an orientation of the exocyclic double bond as shown in Figure S6 of the Supporting Information, in which the distances are very close to the experimental values (2.33 and 2.47 Å, respectively). The NMR-derived conformation is essentially identical with the structure obtained by the computational study.

■ DISCUSSION

Unexpectedly, the ^{1}H and ^{13}C NMR studies under the conditions of reaction as well as the computational study reveal that artemisinate has a single preferred conformation. The NMR studies do not detect any other accessible conformation at 300 K, and therefore, a single conformation dominates at 273 K, which is the temperature of the reaction with diazene. This leads to a simple interpretation of the high selectivity of the reaction with the diazene. The calculations show that the reaction has low activation energies and consequently reactant-like transition states for all values of θ. The preferred transition state has a conformation of the artemisinate fragment similar to free artemisinate. For this preferred conformation, the face of the C2═C3 double bond, which is cis to the decalene group is essentially shaded from any addition of a reagent. Consequently, the diazene approaches from the opposite face, in what could be called an exo attack, and yields **2a** in a large proportion.

The differences in energy between the two key conformers of free artemesinate determine in a large part the difference in

dx.doi.org/10.1021/jo500233z | J. Org. Chem. 2014, 79, 5939−5947

energy between the two transition states that form the two diastereomers. This leads to a rapid reaction that is also stereoselective, two characteristics that are not frequently associated. One key interaction, which stabilizes the conformer (θ = −109°) relative to the other one (θ = 90°), is the noncovalent interaction between the π density of the C2═C3 double bond and the vinylic H7C7 bond. The ELF analysis shows that the C2═C3 π bond is still present at the transition state, which results in the noncovalent $\pi_{C2=C3}$/H7C7 interaction still acting as a stabilizing factor. The structural features at the transition state are coherent with the density analysis: the geometry around C2 and C3 indicates an essentially planar double bond and weak interactions of these two carbons with the two hydrogen atoms originating from the diazene. A rapid reaction, with an almost intact C2═C3 π bond, capable of interacting with the vinylic H7C7 bond, is thus essential for high diastereoselectivity. This leads to the paradoxical result that the reaction is high diastereoselective because it has an early transition state and a low energy barrier associated with a strong exothermicity, characteristics that are usually not beneficial for high selectivity.

This is a case where it would have been difficult to identify the preferred conformation using current chemical intuition and a computational study helps to show that the conformation of $\mathbf{1}_{ate}$ for θ = −109° is more stable than that for θ = 90°. In both conformations, the C2−C4 bond is approximately parallel to the π system of the C2═C3 bond. These conformations are related to those mentioned in the Felkin−Anh rule.[64−66] However, there is no easy way to select which of the two conformations may lead to the major diastereoisomer since there is no direct contact between the cis-decalene group that transfers the chirality information and the incoming reagent. Other factors are at work.

It would have been of great interest to establish a hierarchy of interactions that could contribute to evaluate the preferred conformation. At the present level, it seems very challenging to do so, and there is no obvious way to predict the optimal network of noncovalent interactions. Despite this difficulty, it is interesting to note that a network where all electron donating groups (X = oxygen and $\pi_{C2=C3}$ density) are involved in nonclassical X···HC interactions is preferred to one where one of the electron donating groups, namely the $\pi_{C2=C3}$ bond, is not participating. The result that all electron donor groups could engage in nonclassical X···HC could be a useful guideline for analyzing other structures. A structural analysis of the Cambridge Data Base for detecting of related structural patterns is being undertaken. This study also indicates that diazene could be a very interesting reactant for diastereoselective hydrogenation of double bonds.

CONCLUSION

The high diastereoselectivity of the hydrogenation of artemisinate by diazene to form the desired diastereoisomer of dihydroartemisinate necessary for efficient production of artemisin has been rationalized by state-of-the-art DFT calculations and identification of the noncovalent interactions by coupled ELF/NCI analysis. A single conformer of artemisinate is responsible for the high diastereoselectivity of the reaction. NMR studies in the conditions of reaction confirm the preference for a single conformation that is found to be identical to that predicted by the calculations. The calculations and ELF/NCI analysis show that the lowest transition state and preferred conformation of free artemisinate develop the same network of weak noncovalent interaction within the artemisinate. The reason is that the transition state is reactant-like in agreement with the calculated low energy barrier for hydrogenation. This results in high selectivity for a strongly exothermic reaction even though there is no direct contact between the diazene and the *cis*-decalene derivative of artemisinate that acts as chirality transfer agent. This study could suggest new routes for efficient, rapid, and highly selective hydrogenation.

EXPERIMENTAL SECTION

NMR Studies. *Experiment.* NMR spectra were recorded on a spectrometer operating at a proton frequency of 500.30 MHz and a ^{13}C-carbon frequency of 125.82 MHz. The instrument was equipped with a 5 mm TCI cryo probe head. All experiments were carried out with a sample of 6 mg of artemesinate dissolved in 600 μL of MeOD-d_4 at 300 K (5 mg of 40% NaOD solution have been added). For a complete assignment of proton and carbon resonances, see Table S1 (Supporting Information). 1D-^{1}H, 1D-^{13}C, DQF-COSY, NOESY (mixing time 150 ms), multiplicity edited-HSQC, and HMBC spectra were acquired. ^{1}H and ^{13}C chemical shifts were referenced to TMS.

Two-dimensional homonuclear experiments, DQF-COSY and NOESY, were performed with a spectral width of 7 ppm. Spectra were recorded with 1024 increments in t_1 and 4096 complex data points in t_2. For each t_1 value two (DQF-COSY) or eight (NOESY) transients were averaged, respectively.

For the multiplicity edited HSQC spectrum 1024 increments with 2048 complex data points in t_2 were collected using a sweep width of 7 ppm in the proton and 160 ppm in the carbon dimension. For each t_1 value two transients were averaged. The HMBC spectrum was acquired with a sweep width of 7 ppm in the proton and 200 ppm in the carbon dimension using a defocusing delay of 62 ms (optimized for coupling constants of 8 Hz). A total of 16 transients were averaged for each of 1024 increments in t_1, and 4096 complex points in t_2 were recorded.

Modeling. The 3D-structure of Artemesinate has been determined by restrained molecular dynamics calculations and energy minimization. Molecular dynamics (MD) simulations and interactive modeling were performed using the software package SYBYL, version 2.0. All energy calculations were based on the Tripos force field. For energy minimizations the Powell method was used.

The experimental data set used as input for the MD calculations included 18 distance constraints obtained from a NOESY spectrum recorded in MeOD-d_4 at 300 K (mixing time was 150 ms). The integrals were referenced to the NOE between the geminal protons $H8_{ax}$/$H8_{eq}$ which was set to 1.8 Å. Upper and lower distance limits were set to plus and minus 10% of the calculated (experimental) distances, respectively. For methyl groups, 1.0 Å was added to the upper bound as pseudoatom correction. The set of utilized distance constraints is summarized in Table 2 of the Supporting Information

After an initial energy minimization, the NOE-derived distance constraints were applied with a force constant of 83.74 kJ/mol* Å^2 (20 kcal/mol* Å^2). In the subsequent production run in vacuo at 300 K, conformers were sampled every 1000 ps for a duration of 10 ns yielding a total of 10 structures. The obtained structures were energy-minimized in vacuo with a convergence criterion of 0.21 kJ/ (mol*Å).

ASSOCIATED CONTENT

Supporting Information

Additional information for the NMR study of $\mathbf{1}_{ate}$. Full list of authors for ref 43. Rotational barrier of $\mathbf{1}_{ate}$. Additional energy information associated with Tables 1 and 2. Full size and additional ELF/NCI figures with technical and cutoff information. ELF analysis for $\mathbf{1}_{ate}$ and the transition states corresponding to entries 1 and 6 in Table 1. List of coordinates of all optimized structures. This material is available free of charge via the Internet at http://pubs.acs.org.

dx.doi.org/10.1021/jo500233z | J. Org. Chem. 2014, 79, 5939−5947

AUTHOR INFORMATION

Corresponding Authors

*E-mail: bertrand34130@gmail.com.
*E-mail: robin.chaudret@scienomics.com.
*E-mail: odile.eisenstein@univ-montp2.fr.

Present Address

[#](R.C.) Scienomics 17 Square, Edouard VII 75009, Paris, France.

Notes

The authors declare no competing financial interest.

ACKNOWLEDGMENTS

We thank Dr. Eric Clot for discussions and advice and Dr. Fabrice Boyrie for technical help. B.C. and O.E. thank the CNRS and the Ministère de la Recherche et de l'Enseignement Supérieur for funding. R.C. thanks IFP for a fellowship.

REFERENCES

(1) Gung, B. W.; le Noble, B. *Chem. Rev.* **1999**, *99*, 1067−1068.
(2) (a) Mehta, G.; Chandrasekhar, J. *Chem. Rev.* **1999**, *99*, 1437−1467. (b) Adcock, W.; Trout, N. A. *Chem. Rev.* **1999**, *99*, 1415−1435. (c) Mengel, A.; Reiser, O. *Chem. Rev.* **1999**, *99*, 1191−1223.
(3) Kaselj, M.; Chung, W.-S.; le Noble, W. J. *Chem. Rev.* **1999**, *99*, 1387−1413.
(4) Dannenberg, J. J. *Chem. Rev.* **1999**, *99*, 1225−1241.
(5) Knowles, W. S. *Angew. Chem., Int. Ed.* **2002**, *41*, 1998−2007.
(6) Noyori, R. *Angew. Chem., Int. Ed.* **2002**, *41*, 2008−2022.
(7) Gopailaiah, K.; Kagan, H. B. *Chem. Rev.* **2011**, *111*, 4599−4657.
(8) Gridnev, I. D.; Imamoto, T. *Acc. Chem. Res.* **2004**, *37*, 633−644.
(9) Gridnev, I. D.; Imamoto, T. *Chem. Commun.* **2009**, 7447−7464.
(10) Knowles, W. S.; Noyori, R. *Acc. Chem. Res.* **2007**, *40*, 1238−1239.
(11) Kraft, V.; Kretzschmar, G.; Rossen, K. WO2011030223, Sanofi.
(12) Feth, M. P.; Rossen, K.; Burgard, A. *Org. Process Res. Dev.* **2013**, *17*, 282−293.
(13) Steiner, T. *Angew. Chem., Int. Ed.* **2002**, *41*, 48−76.
(14) Takahashi, O.; Kohno, Y.; Nishio, M. *Chem. Rev.* **2010**, *110*, 6049−6076.
(15) Nishio, M. *Phys. Chem. Chem. Phys.* **2011**, *13*, 13873−13900.
(16) Echeverría, J.; Aullón, G.; Danovich, D.; Shaik, S.; Alvarez, J. *Nature Chem.* **2011**, *3*, 323−330.
(17) Roth, R. J.; Acton, N. *J. Nat. Prod.* **1989**, *52*, 1183−1185.
(18) Bharel, S.; Gulati, A.; Abdin, M. Z.; Srivastava, P. S.; Vishwakarma, R. A.; Jain, S. K. *J. Nat. Prod.* **1998**, *61*, 633−636.
(19) Wong, A.; Goodrich, W. S. WO2006128126 Al *(74)*, 2006.
(20) Covello, P. S. *Phytochemistry* **2008**, *69*, 2881−2885.
(21) Lévesque, F.; Seeberger, P. H. *Angew. Chem., Int. Ed.* **2012**, *51*, 1706−1709.
(22) Kopetzki, D.; Lévesque, D. F.; Seeberger, P. H. *Chem.—Eur. J.* **2013**, *19*, 5450−5456.
(23) http://www.youtube.com/watch?v=7xh8lFHEQDw.
(24) Ro, D. K.; Paradise, M. E.; Ouellet, M.; Fisher, K. J.; Newman, K. L.; Ndungu, J. M.; Ho, K. A.; Eachus, R. A.; Ham, T. S.; Kirby, J.; Chang, M. C.; Withers, S. T.; Shiba, Y.; Sarpong, R.; Keasling, J. D. *Nature* **2006**, *440*, 940−943.
(25) Hale, V.; Keasling, J. D.; Renninger, N.; Diagana, T. T. *Am. J. Trop. Med. Hyg.* **2007**, *77*, 198−202.
(26) Tsuruta, H.; Paddon, C. J.; Eng, D.; Lenihan, J. R.; Horning, T.; Anthony, L. C.; Regentin, R.; Keasling, J. D.; Renninger, N. S.; Newman, J. D. *PloS ONE* **2009**, *4*, e4489.
(27) Paddon, C. J.; Westfall, P. J.; Pitera, D. J.; Benjamin, K.; Fisher, K.; McPhee, D.; Leavell, M. D.; Tai, A.; Main, A.; Eng, D.; Polichuk, D. R.; Teoh, K. H.; Reed, D. W.; Treynor, T.; Lenihan, J.; Fleck, M.; Bajad, S.; Dang, G.; Dengrove, D.; Diola, D.; Dorin, G.; Ellens, K. W.; Fickes, S.; Galazzo, J.; Gaucher, S. P.; Geistlinger, T.; Henry, R.; Hepp, M.; Horning, T.; Iqbal, T.; Jiang, H.; Kizer, L.; Lieu1, B.; Melis, D.; Moss, N.; Regentin, R.; Secrest, S.; Tsuruta, H.; Vazquez, R.; Westblade, L. F.; Xu, L.; Yu, M.; Zhang, Y.; Zhao, L.; Lievense, J.; Covello, P. S.; Keasling, J. D.; Reiling, K. K.; Renninger, N. S.; Newman, J. D. *Nature* **2013**, *496*, 528−532.
(28) Dhainaut, J.; Dlubala, A.; Guevel, R.; Medard, A.; Oddon, G.; Raymond, N.; Turconi, J. WO 2011026365 A1, Sanofi.
(29) Jung, M. *Synlett.* **1990**, 743−744.
(30) Xu, X.-X.; Zhu, J.; Huang, D.-Z.; Zhou, W.-S. *Tetrahedron* **1986**, *42*, 818−829.
(31) Haynes, R. K.; Vonwiller, S. C. *J. Chem. Soc., Chem. Commun.* **1990**, 451−453.
(32) Roth, R. J.; Acton, N. *J. Nat. Prod.* **1989**, *52*, 1183−1185.
(33) Jefford, C. *Adv. Drug Res.* **1997**, *29*, 271−325.
(34) Li, Y.; Wu, Y.-L. *Curr. Med. Chem.* **2003**, 2197−2230.
(35) Han, J. H.; Lee, J. G.; Min, S. S.; Park, S. H.; Angerhofer, C. K.; Cordell, G. A.; Kim, S. U. *J. Nat. Prod.* **2001**, *64*, 1201−1205.
(36) Hünig, S.; Müller, H. R.; Thier, W. *Angew. Chem., Int. Ed.* **1965**, *4*, 271−280.
(37) Pasto, D. J.; Taylor, R. T. Reduction with Diimide. *Org. React.* **2004**, 91−155.
(38) Becke, A. D. *J. Chem. Phys.* **1993**, *98*, 5648−5652.
(39) Lee, C.; Yang, W.; Parr, R. G. *Phys. Rev. B* **1988**, *37*, 785−789.
(40) Grimme, S.; Antony, J.; Ehrlich, S.; Krieg, H. *J. Chem. Phys.* **2010**, *132*, 154104.
(41) Marenich, A. V.; Cramer, C. J.; Truhlar, D. G. *J. Phys. Chem. B* **2009**, *113*, 6378−6396.
(42) Test calculations with SMD optimization, including the D3 correction, do not significantly modify the results.
(43) Frisch, M. J. et al. Gaussian 09, Revision B01, Gaussian, Inc., Wallingford, CT, 2009.
(44) Becke, A. D.; Edgecombe, K. E. *J. Chem. Phys.* **1990**, *92*, 5397−5403.
(45) Silvi, B.; Savin, A. *Nature* **1994**, *371*, 683−686.
(46) Johnson, E. R.; Keinan, S.; Mori-Sanchez, P.; Contreras-Garcia, J.; Cohen, A. J.; Yang, W. T. *J. Am.. Chem. Soc.* **2010**, *132*, 6498−6506.
(47) Pilme, J.; Piquemal, J. P. *J. Comput. Chem.* **2008**, *29*, 1440−1449.
(48) Contreras-Garcia, J.; Johnson, E. R.; Keinan, S.; Chaudret, R.; Piquemal, J.-P.; Beratan, D. N.; Yang, W. *J. Chem. Theory Comput.* **2011**, *7*, 625−632.
(49) Piquemal, J. P.; Pilmé, J.; Parisel, O.; Gérard, H.; Fourré, I.; Bergès, J.; Gourlaouen, C.; De La Lande, A.; Van Severen, M. C.; Silvi, B. *Int. J. Quantum Chem.* **2008**, *108*, 1951−1969.
(50) Chaudret, R.; Cisneros, G. A.; Parisel, O.; Piquemal, J.-P. *Chem.—Eur. J.* **2011**, *17*, 2833−2837.
(51) Wu, P.; Chaudret, R.; Hu, X.; Yang, W. *J. Chem. Theory Comput.* **2013**, *9*, 2226−2234.
(52) Alonso, M.; Geerlings, P.; De Proft, F. *Chem.—Eur. J.* **2013**, *19*, 1617−1628.
(53) Gillet, N.; Chaudret, R.; Contreras-Garcia, J.; Yang, W. T.; Silvi, B.; Piquemal, J.-P. *J. Chem. Theory Comput.* **2012**, *8*, 3993−3997.
(54) Fang, D.; Chaudret, R.; Piquemal, J.-P.; Cisneros, G. A. *J. Chem. Theory Comput.* **2013**, *9*, 2156−2160.
(55) Corey, E. J.; Pasto, P. J.; Mock, W. L. *J. Am. Chem. Soc.* **1961**, *13*, 2957−2958.
(56) Corey, E. J.; Mock, W. L.; Pasto, P. J. *Tetrahedron Lett.* **1961**, *2*, 347−352.
(57) Hünig, S.; Müller, H. R.; Thier, W. *Tetrahedron Lett.* **1961**, *2*, 353−357.
(58) Van Tamelen, E. E.; Dewey, R. S.; Timmons, R. J. *J. Am. Chem. Soc.* **1961**, *83*, 3725−3726.
(59) Fernandez, I.; Cossio, F. P.; Sierra, M. A. *Chem. Rev.* **2009**, *109*, 6687−6711 and references cited therein.
(60) McKee, M. L.; Stanbury, D. M. *J. Am. Chem. Soc.* **1992**, *114*, 3214−3219.
(61) Tang, H. R.; McKee, M. L.; Stanbury, D. M. *J. Am. Chem. Soc.* **1995**, *117*, 8967−8973.
(62) Pasto, D. J.; Chipman, D. M. *J. Am. Chem. Soc.* **1979**, *101*, 2290−2296.

(63) McKee, M. L.; Squillacote, M. E.; Stanbury, D. M. *J. Phys. Chem.* **1992**, *96*, 3266−3272. Correction: McKee, M. L.; Squillacote, M. E.; Stanbury, D. M. *J. Phys. Chem.* **1993**, *97*, 9074.
(64) Chérest, M.; Felkin, H.; Prudent, N. *Tetrahedron Lett.* **1968**, 2199−2204.
(65) Nguyen, T. A.; Eisenstein, O. *Nouv. J. Chim.* **1977**, *1*, 61−70.
(66) For a recent review on the computational studies of asymmetric induction, see: Balcells, D.; Maseras, F. *New J. Chem.* **2007**, *31*, 333−343. For a review on the challenge on computational approach of asymmetric synthesis, see: Brown, J. M.; Deeth, R. J. *Angew. Chem., Int. Ed.* **2009**, *48*, 4476−4479.

■ NOTE ADDED AFTER ASAP PUBLICATION

This paper was published ASAP on March 20, 2014. The data for TS ProS-71 was updated in the Supporting Information and the coordinates are available in .xyz format. The revised paper was reposted on June 24, 2014.